ACS OMEGA

Article

Cite This: ACS Omega 2018, 3, 16831−16838

http://pubs.acs.org/journal/acsodf

Generic Assay of Sulfur-Containing Compounds Based on Kinetics Inhibition of Gold Nanoparticle Photochemical Growth

Anastasia Kostara, George Z. Tsogas,* Athanasios G. Vlessidis, and Dimosthenis L. Giokas*

Department of Chemistry, University of Ioannina, University Campus, 45110 Ioannina, Greece

Supporting Information

ABSTRACT: This work describes a new, equipment-free, generic method for the determination of sulfur-containing compounds that is based on their ability to slow down the photoreduction kinetics of gold ions to gold nanoparticles. The method involves tracking the time required for a red coloration to appear in the tested sample, indicative of the formation of gold nanoparticles, and compare the measured time relative to a control sample in the absence of the target analyte. The method is applicable with minimal and simple steps requiring only two solutions (i.e., a buffer and a gold solution), a source of light (UV or visible), and a timer. The method responds to a large variety of sulfur-containing compounds including thiols, thioesters, disulfides, thiophosphates, metal−sulfur bonds, and inorganic sulfur and was therefore applied to the determination of a variety of compounds such as dithiocarbamate and organophosphorous pesticides, biothiols, pharmaceutically active compounds, and sulfides in different samples such as natural waters and wastewater, biological fluids, and prescription drugs. The analytical figures of merit of the method include satisfactory sensitivity (quantitation limits at the low μM levels), good recoveries (from 93 to 109%), and satisfactory reproducibility (from 4.8 to 9.8%). The method is easily adoptable to both laboratory settings and nonlaboratory conditions for quantitative and semiquantitative analysis, respectively, is user-friendly even for the minimally trained user, and can be performed with limited resources at low cost.

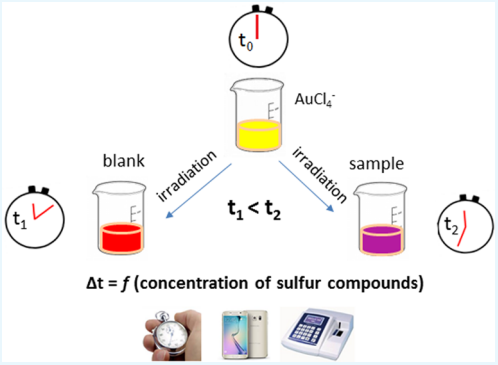

INTRODUCTION

One of the most salient features of noble-metal nanoparticles (NPs) is their ability to undergo intense colorimetric transitions in response to a change in their localized surface plasmon resonance due to size or shape modifications.[1] This property has driven research in the use of nanoparticles as labels for a wide range of optical sensing and analyte-recognition events,[2,3] with improved sensitivity, selectivity, and multiplexing capabilities as compared to conventional molecular probes.[4]

The key to the development of nanoparticle-based optical sensing platforms is to design nanoparticles that disperse or aggregate in the presence of the target analyte.[5] This is usually accomplished by tethering appropriate analyte−receptor molecules on the NPs surface, analyte-mediated removal of stabilizers from the NPs surface, or analyte-driven destruction of interparticle bonds.[6] Another approach is based on the ability of the analytes to modulate the morphological properties of nanoparticles during their formation and, thus, gives rise to specific spectral changes as compared to nanoparticle suspensions prepared in the absence of the analytes. This is accomplished when the target analyte can interact with the precursor (noble) metal ions before they are reduced to NPs. Such examples are the formation and growth of noble-metal NPs as a function of the reducing power of phenolic acids,[7] antioxidant compounds,[8] and b-agonists,[9] the inhibitory effect of DNA bases in the formation of AuNPs due to their strong coordination with gold ions,[10] and the detection of mercury based on the formation of an amalgam between mercury and gold.[11] Enzymatic reactions further expand the scope of analyte-modulated NPs formation by enabling the detection of "inert" analytes that show no affinity for metal nanoparticles or their precursor metal ions.[12] For example, alcohol dehydrogenase has been used to generate nicotinamide adenine dinucleotide phosphate, which can act as a reducing agent, changing the shape and size of AuNPs.[13] In the same line of thinking, oxidase-based biosensors have been employed to mediate the catalytic formation of gold nanoparticles through the reduction of $AuCl_4^-$ by enzymatically produced hydrogen peroxide.[14] Another popular application is the hydrolysis of acetylthiocholine by acetylcholine esterase (AChE) to produce thiocholine, which acts both as a reducing and a capping agent for $AuCl_4^-$ and AuNPs, respectively. Inhibitors of AChE (such as nerve gases or organophosphorous pesticides) can therefore be indirectly determined by measuring the inhibition of acetylthiocholine hydrolysis to thiocholine.[15−18] In all these approaches, a reducing agent, that is either separately added to the solution or produced in situ from the enzymatic reaction of the analyte, is

Received: October 15, 2018
Accepted: November 27, 2018
Published: December 7, 2018

DOI: 10.1021/acsomega.8b02804
ACS Omega 2018, 3, 16831−16838

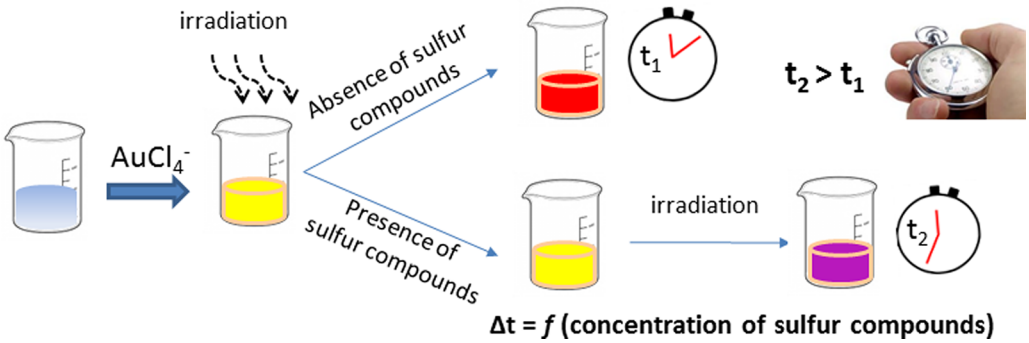

Figure 1. Graphical representation of the general experimental procedure for the time-based assay of sulfur-containing compounds.

necessary to ensure the reduction of noble-metal ions to their respective nanoparticle species.

Except reducing agents, several studies have shown that ultraviolet and visible light can be also used to generate metal nanoparticles in the presence of appropriate molecules that can bind to metal ions and act as photosensitizers.[19−23] However, only a limited number of studies have exploited this principle for the development of new sensing strategies, i.e., using the influence of the target analytes in the photochemical formation of NPs. Most of these studies focus on silver ions due to their easy photoreduction under UV or visible light. For example, Jung et al. (2013) used the photoinduced reduction of silver ion bound to DNA bases for the detection of bacterial genomic DNA.[24] Our group reported the determination of dissolved organic matter in natural waters based on the formation of silver nanoparticles via photostimulated reduction of silver ions by humic and fulvic acids under UV light.[25] Recently, we have also exploited the influence of biothiols in the UV-light-mediated photochemical reduction of silver halide nanocrystals for the determination of biologically relevant thiol species (cysteine, glutathione, and homocysteine) in body fluids.[26] Pu et al. (2018) reported a biomolecule-templated photochemical synthesis of silver nanoparticles and demonstrated its use for the statistical discrimination among different proteins.[27] With regard to gold ions, only one study, to our knowledge, has been reported to exploit the influence of the target analytes in the photochemical reduction of gold ions. Specifically, biothiols were found to inhibit the formation of AuNPs, produced from the combined effect of UV light and tryptophan as the reducing agent. The inhibition was measured spectrophotometrically and used for the determination of thiols in human plasma.[28]

In this work, we report a novel nanotechnology-based method that exploits, for the first time, the kinetics of the photochemical reduction of gold ions to gold nanoparticles for sensing applications. The method is based on recording the time delay in the photoinduced formation of gold nanoparticles in the presence of sulfur-containing compounds using a simple chronometer and the unaided eye as detectors (Figure 1). A wide range of organic and inorganic compounds with different sulfur moieties such as thiols, thioesters, disulfides, thiophosphates, metal−sulfur bonds, and inorganic sulfur were found to slow down the photoreduction kinetics of gold ions both under ultraviolet and visible light. On the basis of this principle, we developed an equipment-free analytical protocol for sulfur-containing compounds and demonstrated its practical utility for a variety of sensing applications.

RESULTS AND DISCUSSION

The formation and controlled synthesis of gold nanoparticles from aqueous gold solutions under the influence of light offers some distinct advantages over chemical reduction (bottom-up) methods:[29] (a) the reduction of gold ions is carried without using strong reducing agents (e.g., borohydride) or harsh conditions (e.g., boiling of the solutions) and (b) irradiation diffuses throughout the entire mass of the solution, thus reduction occurs uniformly under controlled reaction rate. Various light sources have been tested for that purpose (such as UV, sunlight, laser, γ-irradiation), but UV irradiation is the most frequently employed because it matches the absorption band of Au^{3+} (about 323 nm).[20,23]

Previous studies have shown that when $AuCl_4^-$ is irradiated with UV light, Au^{3+} is first excited by the incoming radiation and then reduced to Au^{2+}, which is unstable and disproportionates quickly to form Au^+ and Au^{3+}.[20,23] Then, Au^+ either absorbs another photon and photoreduced to Au^0 or slowly disproprionates to from Au^0 and Au^{2+}. The gold atoms, Au^0, can get together to form gold nuclei and AuNPs, which may further catalyze the disproportionation reactions.[20,23] All these reactions require the presence of an additive, which serves to accelerate or trigger the formation of AuNPs through different chemical routes.[16,17,20,23,29] Surfactants, polymers, ethylene glycol, citrate, etc. have been used as sensitizers of the photochemical reduction of gold ions to AuNPs.

In this work, we report that sulfur-containing compounds can not only affect the photochemical formation and growth of AuNPs but also slow down the photoreduction kinetics of AuNPs formation. Figure 2 and the respective UV−vis absorbance spectra (inset graphs) show the kinetics of the photochemical formation of AuNPs under UV light irradiation in the absence and presence of cysteine as a model sulfur-containing compound. A video demonstration of the process in an aqueous solution containing 50.0 μM of cysteine under ambient daylight is given in the Supporting Information (the video is at actual speed but cropped from 1:43 to 3.06 min). All the experiments were carried out in the presence of citrate, which was necessary to sensitize and accelerate the photoreduction of gold to AuNPs because no AuNPs were formed in the absence of citrate, even at longer irradiation times, i.e., >30 min under 40 W of irradiation at 254 nm. Citrate could sensitize the photochemical formation of AuNPs either due to the photoreduction of citrate to acetone-1,3-dicarboxylate and free electrons, which reduce Au^{m+} (m = 1, 2, 3) to Au^0 or due to the direct excitation of the citrate−Au^{3+} complex that could reduce Au^{3+} through electron-transfer mechanisms.[23]

DOI: 10.1021/acsomega.8b02804
ACS Omega 2018, 3, 16831−16838

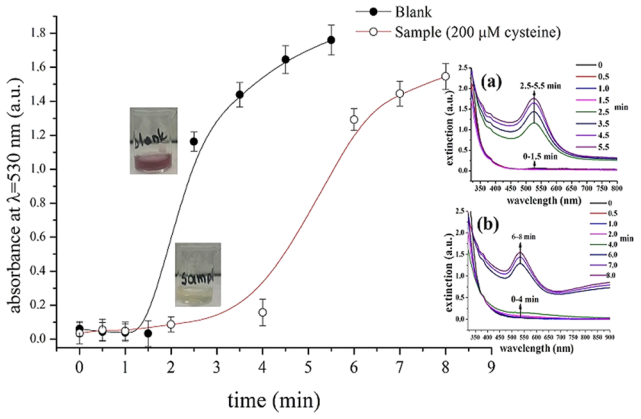

Figure 2. Kinetics of AuNPs photochemical formation in the absence and presence of 200.0 μM cysteine. Inset graphs show the respective UV−vis spectra at different time intervals (a) UV−vis spectra of AuNPs formation in the absence of cysteine and (b) UV−vis spectra in the presence of 200.0 μM cysteine. Experimental conditions: pH 4 (citrate citric acid buffer, 8.0 mM), λ = 254 nm, and 40 W.

Optimization of Gold Photoreduction. The photochemical formation and growth of AuNPs from gold chloride solutions is a kinetic phenomenon that continues even after exposure to irradiation has been stopped. Depending on the experimental conditions (intensity of UV irradiation, concentration of gold ions, presence of additives, etc.), the formation and growth of AuNPs may continue for several hours after stopping the irradiation until reaching an equilibrium.[20] This phenomenon is not a limitation in our time-based assay because the analytical signal is the time required for a colored solution to appear; once the color becomes evident, the formation of AuNPs is no longer monitored. To optimize the experimental conditions of the assay, however, we used the absorbance of the solutions to obtain (absorbance) measurements at a fixed time for all optimization experiments. Therefore, the influence of incubation time (after UV irradiation has been stopped) was the first parameter investigated. We measured the absorbance of the blank and sample solutions at 525 nm after exposure for 1.5 min under UV light (254 nm, 40 W) and incubation in the dark at room temperature for various time intervals. We irradiated the samples for 1.5 min because according to the kinetic curves of Figure 2, both the sample and the blank solutions show no significant increase in the absorbance values, whereas at longer irradiation times, the absorbance of the blank increases abruptly. In addition, the samples were kept in dark to avoid exposure to ambient light, which can also induce the photoreduction of $AuCl_4^-$.[21] According to the results of Figure 3a, the net analytical signal (i.e., absorbance intensity of the sample minus the absorbance intensity of the blank solution) increases rapidly

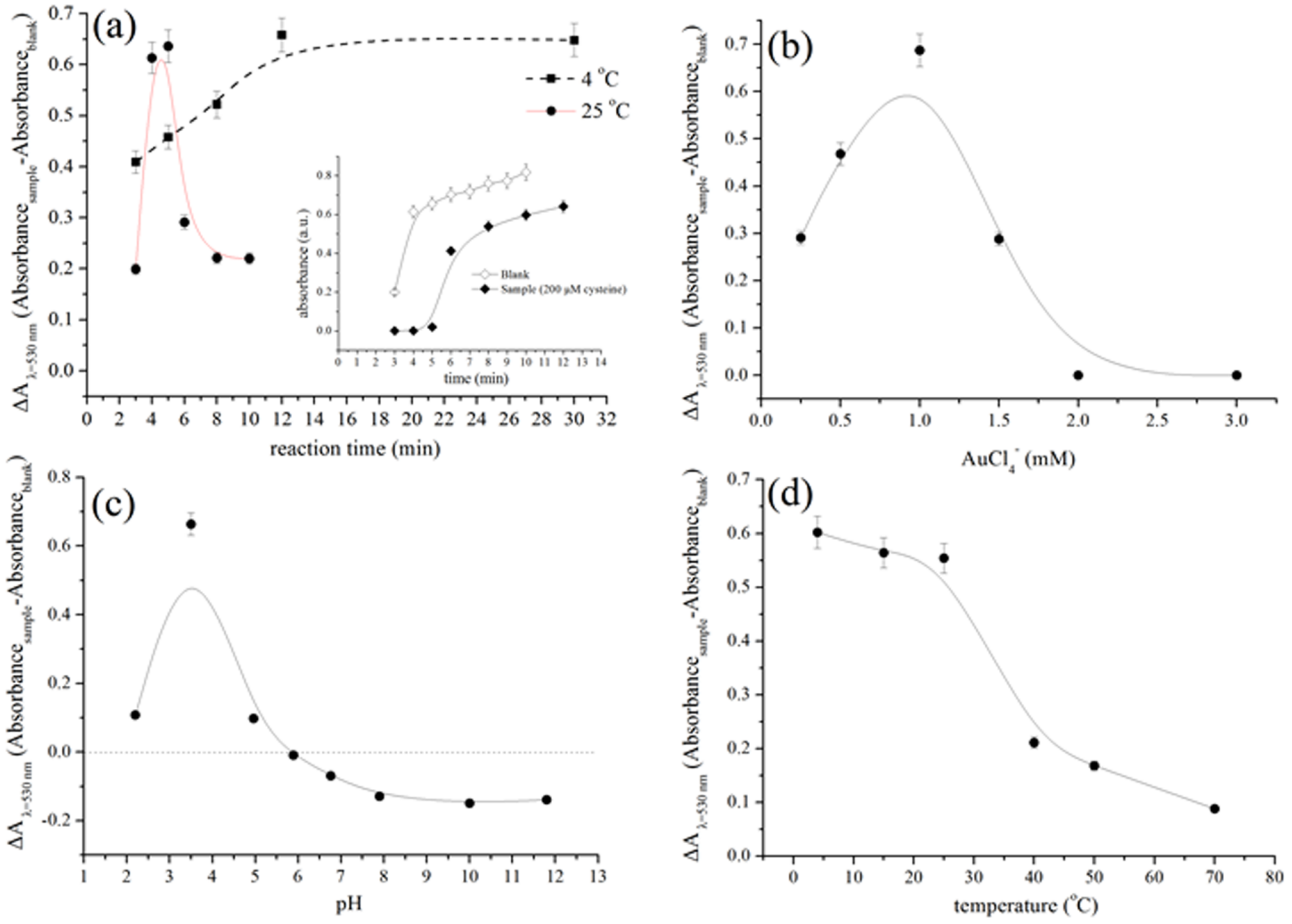

Figure 3. Optimization of gold photoreduction in the presence of 50.0 μM cysteine as a model sulfur-containing compound and citrate as photosensitizer at λ = 254 nm (40 W). Effects of (a) reaction time in the dark (after UV irradiation), (b) $AuCl_4^-$ concentration, (c) solution pH, and (d) temperature on the net absorbance signal intensity (ΔA) calculated as the difference between the absorbance signal of the sample and the absorbance signal of the blank at λ = 530 nm.

DOI: 10.1021/acsomega.8b02804
ACS Omega 2018, 3, 16831−16838

after 5 min of incubation at room temperature (~25 °C) but dramatically decreases at longer times. This pattern is obtained due to the faster formation of AuNPs in the blank sample in the first 4 min of incubation, whereas in the presence of cysteine, the formation of AuNPs slows down and becomes apparent only after 6 min (Figure 3a, inset); hence, the difference in the net absorbance value reaches its maximum after 5 min and decreases thereafter. When the same experiments were performed in cold conditions (i.e., 4 °C), the reaction rate decreased and the absorbance signal reached its maximum value after 12 min of incubation. These data suggest that temperature also affects the kinetics of gold photoreduction. On the basis of these findings, all the absorbance measurements were performed under fixed conditions that involve exposure to UV light (40 W, 254 nm) for 1.5 min and incubation at room temperature protected from ambient light exposure for 5 min.

Following the optimization of reaction kinetics, we studied the influence of $AuCl_4^-$ and citrate concentration, pH, temperature, and wavelength of irradiation. The results of Figure 3b show that the net absorbance signal increases significantly at $AuCl_4^-$ concentration up to 1.0 mM due to a significant increase in the absorbance of the blank solution (not shown). At higher gold concentrations, the absorbance decreases dramatically for both the sample and the blank solutions possibly because a higher amount of energy is required to photoreduce the large concentration of gold ions. Therefore, 1 mM of $AuCl_4^-$ was used throughout the experiments.

The concentration of citrate ions, necessary to sensitize the photochemical reduction of gold ions was found to depend on light intensity. A higher amount of citrate was required with decreasing light intensity (i.e., increasing irradiation wavelength). In the working conditions (40 W of light intensity at 254 nm, in the presence of 50.0 μM of cysteine), the optimum citrate ion concentrations was 5.0 mM, whereas at higher citrate concentrations, the net absorbance signal intensity declined possibly because citrate accelerated the photoreduction of gold ion solutions.[23]

With regard to pH, the acidic values (pH 3.5) were found to produce the best results (Figure 3c). As the pH increases above the optimum (pH $\geq$ 3.5), the net absorbance signal intensity exhibits a behavior, which seems to be related to the pK_a of the predominant cysteine species. Specifically, the signal decreases to zero at pH 5, which is close to the isoelectric point of cysteine (i.e., 5.14) and the pK_a of citric acid (i.e., 4.74). Then, the signal is reversed (i.e., the absorbance signal intensity of the sample is higher than the absorbance signal intensity of the blank) and gradually decreases up to the value of pH 8.0, which coincides with the acid dissociation constant of the sulfhydryl group (pK_{a2} = 8.18). At pH above 8, the signal remains relatively stable. The fact that the signal of the sample becomes higher than that of the blank at pH values higher than 5 may suggest that photoreduction of $AuCl_4^-$ ions is enhanced in the presence of charged species of cysteine and citrate probably due to ligand-to-metal charge transfer reactions with the predominant gold species at these pH values (possibly $[AuCl(OH)_3]^-$ and $[Au(OH)_4]^-$).[30]

Temperature was also found to play a significant role in the photoreduction of $AuCl_4^-$, both in the presence and the absence of cysteine (Figure 3d). When the samples were irradiated at temperatures higher than room temperature, the net analytical signal (ΔA at λ = 530 nm) decreased, suggesting that temperature accelerated the reduction of $AuCl_4^-$ ions. We attributed these observations to the presence of citrate, which is known to be an efficient reducing agent of gold at elevated temperatures. Therefore, all the experiments were performed at room temperature.

We then sought the optimum wavelength of irradiation at wavelengths in the UV region (254, 312, and 365 nm) and under visible light (i.e., artificial and room light). We observed that the photoreduction was feasible at all wavelengths, including ambient light, but longer irradiation times were required with increasing wavelength (i.e., lower intensity). For example, the formation of AuNPs in the presence of 200.0 μM cysteine at room temperature and 40 W of UV irradiation at 254 nm was evident after 6 min (Figure 2). When the same experiment was performed under room light, it needed more than 1 h to obtain a measurable signal. The experimental conditions and the selected (optimum) values are summarized in Table S1.

Effect of UV Intensity. The influence of irradiation intensity (from 8 to 40 W at 254 nm) as a function of cysteine concentration was investigated under the optimum experimental conditions using time as a metering unit. We monitored the formation of AuNPs with the unaided eye (against a white background to facilitate the observation of the colorimetric changes) and recorded the time required for a colored solution to appear in the blank and the sample solutions. The timer was manually started with exposure to irradiation and stopped upon the appearance of a faint red−purple coloration indicative of the formation of AuNPs. The time required for a colored solution to appear as a function of cysteine concentration and for different UV intensities is shown in Figure S1. These results show that (a) the irradiation time, necessary for AuNPs to produce an optically observable coloration, decreases with increasing UV intensity and (b) the kinetics of AuNPs formation follow a linear pattern with increasing cysteine concentration. We also observed that the sensitivity of the method changes with irradiation intensity; at lower light intensity (8 and 16 W), the method exhibits higher sensitivity, whereas at higher light intensity (24, 32 and 40 W), the sensitivity decreases. Therefore, we concluded that any irradiation intensity can be employed for the measurements, but dilute samples (containing low concentrations of sulfur-containing compounds) can be more conveniently analyzed using lower UV intensities to enable easier discrimination and measurement of time. On the other hand, concentrated samples (that contain high concentrations of sulfur-containing compounds) can be analyzed under higher UV intensity to accelerate the photoreduction kinetics and reduce the analysis time.

Timing and Signal Acquisition. Although observations with the unaided eye are simple to perform, they are not practical for stand-alone applications because the user's attention must be fixed on the assay while it is running, so a user cannot do multitasking, e.g., analyzing multiple samples or running other tests in parallel, is not possible. In addition, it requires observation of colorimetric changes, which may be influenced by the experience of the user or its ability to perceive color. In these cases, the method may be limited to semi-quantitative measurements. Coupling the time-based readout with a digital camera for the measurement of the run time of the assay can be used to overcome these limitations and provide a more accurate timing of the observed colorimetric transitions.

To compare the accuracy of the measurements between manual and video timing, we prepared a calibration plot with increasing cysteine concentration from 0 to 200 μM and recorded the time delay in the formation of AuNPs both manually (with the unaided eye as detector) and with a use of mobile phone camera. Video inspection enabled us to monitor the assay time more easily because it did not require continues

DOI: 10.1021/acsomega.8b02804
ACS Omega 2018, 3, 16831−16838

supervision of the reactions, but the calculated net signal response (i.e., time delay between the blank and the sample solutions) was similar to that recorded by the unattended eye because in both methods, the change in the color of the solutions was observed optically by eye inspection. To minimize user intervention and accomplish more accurate timing, we obtained video stills (as jpeg images) at different time intervals and measured the color intensity (as RGB values) in each image using digital image colorimetry. Figure 4 shows the mean gray

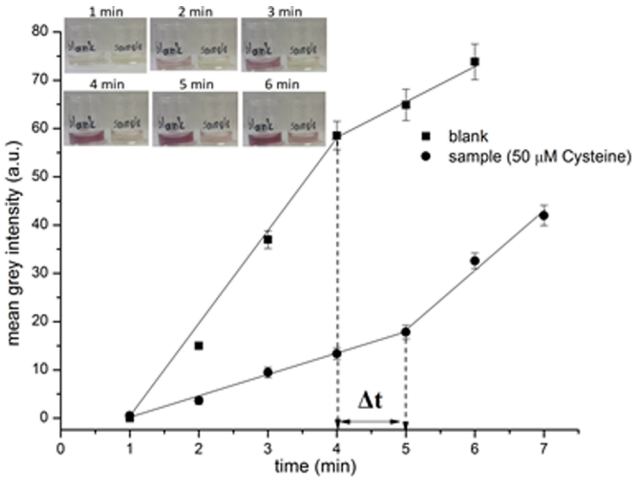

Figure 4. Kinetics of AuNPs photochemical formation as determined using digital image colorimetry. Inset photo: images at time intervals of 1 min.

intensity obtained from the digital images (using the Image J software) at equally spaced time intervals of 1 min for the blank and a sample solution. The change in the slope of the curves signifies the formation of AuNPs and the distance on the x-axis the net signal response (i.e., the time delay in the formation of AuNPs in the blank and the sample solution). As we can observe, the time delay in the formation of AuNPs is calculated to be 1 min, which is higher than that observed with the unaided eye (i.e., 0.6 min). Therefore, this approach could increase the usability of the time-based approach in some settings and provide some improvement to both sensitivity and reproducibility.

Response to Sulfur-Containing Compounds and Selectivity. The kinetics of the photochemical reduction of gold ions in the presence of various sulfur-containing compounds was investigated by irradiating aqueous $AuCl_4^-$ solutions containing 5.0 mM of citrate as photosensitizer. The obtained dose−response plots (time vs concentration) are shown in Figure 5 for a variety of sulfur-containing compounds such as pesticides (dithiocarbamates and organophosphorous), biothiols (cysteine, glutathione, and homocysteine), sulfur-containing drugs (inhibitors of metallo-lactamases), and sulfide ions. All these compounds contain a variety of sulfur-containing moieties (see Table S2), which can bind to gold or gold nanoparticles such as thiols (S−H), thioesters (P−S), disulfides (S−S), metal−sulfur bonds (Me−S), sulfide (S^{2-}), and thiophosphates (P═S) (the latter bonds are able to interact weakly with metal ions via coordinative interactions).[31,32] The analytical figures of merit for each compound (detection limits, repeatability, and linear range) are also gathered in Table S2. With the exception of pesticides, which typically exist at lower concentration levels in environmental samples, the method offers adequate sensitivity for the determination of sulfur-containing compounds in a variety of samples without the need for separate extraction or preconcentration steps.

From the above discussion, it is made clear that the method is not selective for a specific class of sulfur-containing compounds, but it may respond to a variety of compounds containing sulfur moieties. However, each sample matrix may contain a different class of compounds. For example, the predominant sulfur-containing compounds in biological fluids are aminothiols, whereas environmental samples may contain dithiocarbamate and organophosphorous pesticides. In that regard, the method can be used to selectivity determine the total concentration of a specific class of compounds in the tested sample. This is typical in all the assays that are based on the colorimetric changes induced in AuNP suspensions by sulfur-containing compounds. Moreover, from the slopes of the calibration plots of Figure 5 and Table S2, it can be inferred that the analytical response to each sulfur-containing compound is not identical. This observation could be used to qualitatively discriminate among different sulfur-containing compounds in a tested sample. For example, the slopes of the calibration curves for organophosphorous and dithiocarbamate pesticides are different for each pesticide category, thus enabling to obtain a qualitative evidence of the presence of either pesticides species in the real samples. Similarly, the method could be used to assess the authenticity of drugs by comparing the slope of the curve obtained with a standard pharmaceutical compound or a genuine drug to that of an unknown drug sample (using variable dilutions of both the standard and the unkown samples to obtain different concentration levels), and obtain qualitative evidence of the adulteration of the active ingredient or the presence of counterfeit additives. With regard to biothiols, the calibration functions of cysteine and homocysteine, which are the most abundant aminothiol species in blood plasma (150−300 and 5−15 μM, respectively),[33] have similar slope and intercept values; therefore, the total concentration of cysteine and homocysteine can be determined from one calibration function without the loss of accuracy. Further improvement in selectivity can be accomplished by means of appropriate extraction methods, which can relieve the sample from coexisting species and imbue the assay with a high selectivity against a specific class of compounds or analytes.[34]

Selectivity is also influenced by the matrix of the sample. Because the method employs Au ions and light to accomplish the photochemical formation of AuNPs, selectivity may be influenced by coexisting species that may complex Au ions or absorb the incident irradiation. This may affect the selectivity of the assay and produce false-positive or false-negative results. A specific experimental protocol, depending on the sample matrix, was therefore optimized and developed for each analyte and sample matrix. Details from the optimization study and the optimized experimental procedure for each analyte and sample matrix are given in the Supporting Information.

Method Application and Validation. The utility of the method in the analysis of the real samples was examined for (a) the determination of sulfur-containing active ingredients in drugs, (b) the determination of total biothiols in artificial body fluids, (c) the determination of pesticides in environmental waters, and (d) the determination of sulfide in treated wastewater samples. The results from the analysis of different samples for various sulfur-containing compounds are gathered in Table 1. The recoveries were lying between 93 and 109% depending on the sample matrix and target analytes with good

DOI: 10.1021/acsomega.8b02804
ACS Omega 2018, 3, 16831−16838

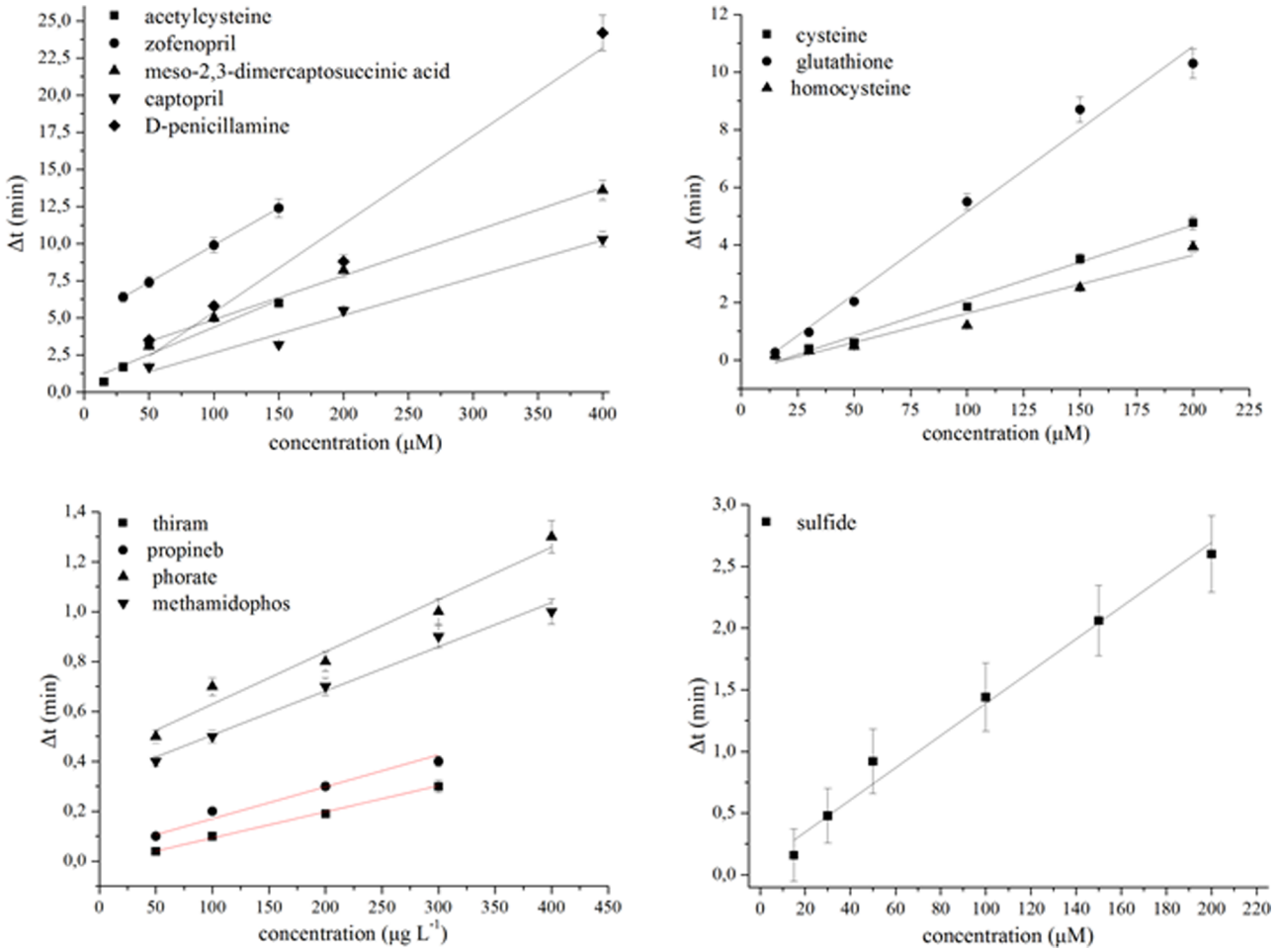

Figure 5. Calibration plots for various sulfur-containing compounds. All the curves were obtained at 40 W irradiation intensity at $\lambda = 254$ nm except for the thiram curve, which was obtained at 8 W ($\lambda = 254$ nm), and the sulfide curve, which was obtained under artificial light in a pooled water sample prepared by mixing four commercial bottled waters.

Table 1. Application of the Method to the Determination of Sulfur-Containing Compounds in Different Matrices and Results from Recovery Experiments

compound	true value	measured	recovery (%)	RSD (%, $n = 5$)
Sulfur-Containing Drugs (μM)[a]				
acetylcysteine	30	28.7	95.6	4.8
	100	97.2	97.2	5.6
captopril	75	81.7	108.9	6.4
	150	157.6	105.1	6.9
Pesticides (μg L^{-1})[b]				
thiram	50	51.0	102.0	7.7
	100	98.5	98.5	7.6
methamidophos	50	46.5	93.0	6.8
	100	94.7	94.7	6.5
Biothiols (μM)[c]				
cysteine	30	28.7	95.6	6.6
	75	73.0	97.3	5.7
Inorganic Sulfur (μM)[d]				
sulfide	15	15.6	104.0	8.9
	50	51.9	103.6	9.8

[a]Commercial drugs. [b]Methanol extracts. [c]Artificial urine solution (AUS). [d]Treated wastewater.

reproducibility. These data indicate that the developed assay can be reliably used for the instrument-free determination of a variety of sulfur-containing compounds in different matrices using a simple chronometer and the unaided eye as detectors.

CONCLUSIONS

In this work, we have described the development of a new nanotechnology-based approach that uses, for the first time, the inhibitory effect of sulfur-containing compounds in the kinetics of the photochemical formation of AuNPs. The method involves tracking the time required for AuNPs to appear in the tested sample, compared to that in a blank solution. On the basis of this principle, a general analytical protocol was devised and appropriately modified for each sample matrix and target analyte to enable the determination of a wide variety of sulfur-containing compounds of environmental, pharmaceutical, and biological interest. The experimental protocol (and its modifications) described herein are simple to perform and do not require instrumental detectors because they can be operated by the unaided eye using a simple timer. The only requirement is the ability of the user to see color and/or the ability to count (i.e., time) to measure the quantity of the analyte. The method could be fieldable because it does not require an external light source; ambient light is well suited for triggering the photochemical formation of AuNPs. The use of a camera can integrate multitasking capabilities and further improve the accuracy and the reproducibility of the measurements.

DOI: 10.1021/acsomega.8b02804
ACS Omega 2018, 3, 16831−16838

EXPERIMENTAL SECTION

Reagents. All the reagents were of analytical grade unless otherwise stated. Hydrogen tetrachloroaurate trihydrate (min. 99.9%), PESTANAL analytical standards of dithiocarbamate fungicides (Thiram and Propineb) and organophosphate pesticides (Phorate and Methamidophos), zofenopril calcium, arginine, asparagine, aspartic acid, L-cysteine, cystine, DL-homocysteine, glutamine, glutamic acid, ammonium chloride, lactic acid, magnesium sulfate, magnesium chloride hexahydrate, sodium sulfide, sodium chloride, sodium sulfate, sodium bicarbonate, dipotassium hydrogen phosphate, potassium dihydrogen phosphate, citric acid, tri-sodium citrate, potassium chloride, calcium chloride dehydrate, uric acid, D(+)-glucose, and creatinine were obtained from Sigma-Aldrich (Steinheim, Germany). L-Glutathione (reduced), meso-2,3-dimercaptosuccinic acid, D-(−)-penicillamine, *N*-acetyl-L-cysteine, and captopril were obtained from Alfa Aesar (Karlsruhe, Germany). Glycine, histidine, lysine, and valine were supplied by Serva Electrophoresis GmbH (Heidelberg, Germany). Finally, urea (>99.5%) was purchased from Pharmacia Biotech AB (Uppsala, Sweden) and HPLC-grade solvent from Fischer Scientific (Loughborough, U.K.).

Equipment. We used a UV illumination chamber (Vilber Lourmat Bio-Link BLX Crosslinker) (4 W cm^{-2}) to illuminate the solutions with UV light (254, 312, and 365 nm) and artificial light (Cool White tubes, 4000 K). The chamber ensures a constant and controlled exposure of the solutions to light throughout the experiments. We captured a video of the overall process using a SAMSUNG S6 Edge mobile phone camera (16.0 Mpixel). Video stills at time intervals of 1.0 min were saved in JPEG format (300 dpi). We measured the mean intensity of the colored solutions in gray scale using Image J software (US National Institute of Health). We measured the signal intensity in gray scale because it was the simplest approach to acquire the analytical signal and avoid data manipulation as well as user intervention. To obtain absorbance measurements, we used matched quartz cells of 1 cm path length in a Jenway (Essex, U.K.) 6405 UV/vis spectrophotometer.

General Experimental Procedure. For all the sulfur-containing compounds, the general experimental procedure involves the sequential addition of 5.0 mM citric acid−sodium citrate buffer pH 3.5 and 1.0 mM $AuCl_4^-$ into an aliquot of the sample to prepare a solution with a final volume of 2 mL. A blank solution containing distilled water, instead of the sample, is prepared in parallel. Both the blank and the sample solutions are irradiated simultaneously under UV or visible light against a white background to facilitate the observation of color development. All the reactions take place at room temperature with no heat detected through feel when the solutions are removed from the irradiation source. The formation of AuNPs is inspected by the unaided eye or a camera operating in video mode. The time delay between the formation of a red−purple coloration in the blank and the sample solutions, indicative of the formation of AuNPs, is used as analytical signal and correlated to the concentration of sulfur-containing species in the sample. A graphical layout of the general experimental procedure is shown in Figure 1.

Depending on the target analyte and the sample matrix composition, some modifications to the general experimental procedure are necessary. The detailed experimental procedure for each sulfur-containing compound and sample matrix is given in the Supporting Information.

Samples. Commercial drugs in different forms (tab, powder, or cap) were purchased from local pharmacies and dissolved in the appropriate solvent (water for acetylcysteine, D-penicillamine, and DL-captopril, dimethyl sulfoxide for zofenopril, and ethanol for meso-2,3-dimercaptosuccinic acid) under stirring and ultrasound irradiation. The solutions were then filtered to remove undissolved excipients and diluted as appropriate with distilled water. Treated wastewater was obtained from the local wastewater treatment plant and filtered through a 0.45 μm filter to remove suspended solids. Bottled waters were obtained from local stores and used as purchased. Artificial urine solution (AUS) was prepared by mixing 1.1 mM lactic acid, 170.0 mM urea, 25.0 mM sodium bicarbonate, 2.0 mM citric acid, 2.5 mM calcium chloride, 90.0 mM sodium chloride, 25.0 mM ammonium chloride, 10.0 mM sodium sulfate, 2.0 mM magnesium sulfate, 7.0 mM dipotassium hydrogen phosphate, and 7.0 mM potassium dihydrogen phosphate in distilled water and adjusting the pH at the value of 6.0.[35] Standard cysteine solution was added to yield a final concentration of 200.0 μM and mixed under stirring for 5 min.

ASSOCIATED CONTENT

Supporting Information

The Supporting Information is available free of charge on the ACS Publications website at DOI: 10.1021/acsomega.8b02804.

Video demonstration of the time-based assay under ambient daylight (AVI)

Experimental variables affecting the photochemical formation of AuNPs; effect of UV light intensity; analytical figures of merit; experimental protocols for the determination of sulfur-containing compounds (determination of sulfur-containing compounds in drugs; determination of biothiols in body fluids; determination of sulfur-containing pesticides; determination of sulfide) (PDF)

AUTHOR INFORMATION

Corresponding Authors

*E-mail: gtsogas@cc.uoi.gr. Tel: +302651008402 (G.Z.T.).
*E-mail: dgiokas@cc.uoi.gr (D.L.G.).

ORCID

Dimosthenis L. Giokas: 0000-0002-1816-5810

Notes

The authors declare no competing financial interest.

REFERENCES

(1) Rycenga, M.; Cobley, C. M.; Zeng, J.; Li, W.; Moran, C. H.; Zhang, Q.; Qin, D.; Younan Xia, Y. Controlling the Synthesis and Assembly of Silver Nanostructures for Plasmonic Applications. *Chem. Rev.* **2011**, *111*, 3669−3712.

(2) Saha, K.; Agasti, S. S.; Kim, C.; Li, X.; Rotello, V. M. Gold Nanoparticles in Chemical and Biological Sensing. *Chem. Rev.* **2012**, *112*, 2739−2779.

(3) Doria, G.; Conde, J.; Veigas, B.; Giestas, L.; Almeida, C.; Assuncao, M.; Rosa, J.; Baptista, P. V. Noble metal nanoparticles for biosensing applications. *Sensors* **2012**, *12*, 1657−1687.

(4) Tansil, N. C.; Gao, Z. Nanoparticles in biomolecular detection. *Nano Today* **2006**, *1*, 28−37.

(5) Ghosh, S. K.; Pal, T. Interparticle Coupling Effect on the Surface Plasmon Resonance of Gold Nanoparticles: From Theory to Applications. *Chem. Rev.* **2007**, *107*, 4797−4862.

(6) Zhao, W.; Brook, M. A.; Li, Y. Design of Gold Nanoparticle-Based Colorimetric Biosensing Assays. *ChemBioChem* **2008**, *9*, 2363−2371.

DOI: 10.1021/acsomega.8b02804
ACS Omega 2018, 3, 16831−16838

(7) Scampicchio, M.; Wang, J.; Blasco, A. J.; Arribas, A. S.; Mannino, S.; Escarpa, A. Nanoparticle-Based Assays of Antioxidant Activity. *Anal. Chem.* **2006**, *78*, 2060−2063.
(8) Choleva, T. G.; Kappi, F. A.; Giokas, D. L.; Vlessidis, A. G. Paper-based assay of antioxidant activity using analyte-mediated on-paper nucleation of gold nanoparticles as colorimetric probes. *Anal. Chim. Acta* **2015**, *860*, 61−69.
(9) He, P.; Shen, L.; Liu, R.; Luo, Z.; Li, Z. Direct Detection of *β*-Agonists by Use of Gold Nanoparticle-Based Colorimetric Assays. *Anal. Chem.* **2011**, *83*, 6988−6995.
(10) Pan, H.; Li, D.; Liu, J.; Li, J.; Zhu, W.; Zhao, Y. Sensing Thermally Denatured DNA by Inhibiting the Growth of Au Nanoparticles: Spectral and Electrochemical Studies. *J. Phys. Chem. C* **2011**, *115*, 14461−14468.
(11) Rex, M.; Hernandez, F. E.; Campiglia, A. D. Pushing the Limits of Mercury Sensors with Gold Nanorods. *Anal. Chem.* **2006**, *78*, 445−451.
(12) Willner, I.; Baron, R.; Willner, B. Growing Metal Nanoparticles by Enzymes. *Adv. Mater.* **2006**, *18*, 1109−1120.
(13) Xiao, Y.; Pavlov, V.; Levine, S.; Niazov, T.; Markovitch, G.; Willner, I. Catalytic growth of Au nanoparticles by NAD(P)H cofactors: Optical sensors for NAD(P)+-dependent biocatalyzed transformations. *Angew. Chem., Int. Ed.* **2004**, *43*, 4519−4522.
(14) Zayats, M.; Baron, R.; Popov, I.; Willner, I. Biocatalytic Growth of Au Nanoparticles: From Mechanistic Aspects to Biosensors Design. *Nano Lett.* **2005**, *5*, 21−25.
(15) Willner, I.; Baron, R.; Willner, B. Growing Metal Nanoparticles by Enzymes. *Adv. Mater.* **2006**, *18*, 1109−1120.
(16) Virel, A.; Saa, L.; Pavlov, V. Modulated Growth of Nanoparticles. Application for Sensing Nerve Gases. *Anal. Chem.* **2009**, *81*, 268−272.
(17) Coronado-Puchau, M.; Saa, L.; Grzelczak, M.; Pavlov, V.; Liz-Marzán, L. M. Enzymatic modulation of gold nanorod growth and application to nerve gas detection. *Nano Today* **2013**, *8*, 461−468.
(18) Lu, L.; Xia, Y. Enzymatic reaction-modulated gold nanorod end-to-end self-assembly for ultrahigh sensitively colorimetric sensing of cholinesterase and organophosphate pesticides in human blood. *Anal. Chem.* **2015**, *87*, 8584−8591.
(19) Jana, J.; Acharyya, P.; Negishi, Y.; Pal, T. Evolution of Silver-Mediated, Enhanced Fluorescent Au−Ag Nanoclusters under UV Activation: A Platform for Sensing. *ACS Omega* **2018**, *3*, 3463−3470.
(20) Eustis, S.; Hsu, H. Y.; El-Sayed, M. A. Gold Nanoparticle Formation from Photochemical Reduction of Au^{3+} by Continuous Excitation in Colloidal Solutions. A Proposed Molecular Mechanism. *J. Phys. Chem. B* **2005**, *109*, 4811−4815.
(21) Dong, S. A.; Zhou, S. P. Photochemical synthesis of colloidal gold nanoparticles. *Mater. Sci. Eng., B* **2007**, *140*, 153−159.
(22) Wang, L.; Wei, G.; Guo, C.; Sun, L.; Sun, Y.; Song, Y.; Yang, T.; Li, Z. Photochemical synthesis and self-assembly of gold nanoparticles. *Colloids Surf., A* **2008**, *312*, 148−153.
(23) Yang, S.; Wang, Y.; Wang, Q.; Zhang, R.; Ding, B. UV irradiation induced formation of Au nanoparticles at room temperature: The case of pH values. *Colloids Surf., A* **2007**, *301*, 174−183.
(24) Jung, Y. L.; Jung, C.; Park, J. H.; Kim, M. I.; Park, H. G. Direct detection of unamplified genomic DNA based on photo-induced silver ion reduction by DNA molecules. *Chem. Commun.* **2013**, *49*, 2350.
(25) Gatselou, V. A.; Giokas, D. L.; Vlessidis, A. G. Determination of dissolved organic matter based on UV-light induced reduction of ionic silver to metallic nanoparticles by humic and fulvic acid. *Anal. Chim. Acta* **2014**, *812*, 121−128.
(26) Kappi, F. A.; Papadopoulos, G. A.; Tsogas, G. Z.; Giokas, D. L. Low-cost colorimetric assay of biothiols based on the photochemical reduction of silver halides and consumer electronic imaging devices. *Talanta* **2017**, *172*, 15−22.
(27) Pu, F.; Ran, X.; Guan, M.; Huang, Y.; Ren, J.; Qu, X. Biomolecule-templated photochemical synthesis of silver nanoparticles: Multiple readouts of localized surface plasmon resonance for pattern recognition. *Nano Res.* **2018**, *11*, 3213−3221.
(28) Jung, Y. L.; Park, J. H.; Kim, M. I.; Park, H. G. Label-free colorimetric detection of biological thiols based on target-triggered inhibition of photoinduced formation of AuNPs. *Nanotechnology* **2016**, *27*, No. 055501.
(29) Dong, S.; Tang, C.; Zhou, H.; Zhao, H. Photochemical Synthesis of Gold Nanoparticles by the Sunlight Radiation using a Seeding Approach. *Gold Bull.* **2004**, *37*, 187−195.
(30) Pacławski, K.; Sak, T. Kinetics and mechanism of the reaction of Gold(III) chloride complexes with formic acid. *J. Min. Metall., Sect. B* **2015**, *51*, 133−142.
(31) Andrews, D. L.; Gaburro, Z. *Frontiers in Surface Nanophotonics: Principles and Applications*, Springer Series in Optical Sciences; Springer, 2007; Vol. *133*, p 171.
(32) Yang, L.; Zhang, X.; Li, H.; Jiang, L. A simple strategy for selective detection of phosphorothiolate pesticides using a hyaluronan-tyrosine gold nanoparticle probe. *Anal. Methods* **2017**, *9*, 6139−6147.
(33) Kappi, F. A.; Tsogas, G. Z.; Routsi, A.-M.; Christodouleas, D. C.; Giokas, D. L. Paper-based devices for biothiols sensing using the photochemical reduction of silver halides. *Anal. Chim. Acta* **2018**, 89−96.
(34) Giannoulis, K. M.; Giokas, D. L.; Tsogas, G. Z.; Vlessidis, A. G. Ligand-free gold nanoparticles as colorimetric probes for the non-destructive determination of total dithiocarbamate pesticides after solid phase extraction. *Talanta* **2014**, *119*, 276−283.
(35) Brooks, T.; Keevil, C. W. A simple artificial urine for the growth of urinary pathogens. *Lett. Appl. Microbiol.* **1997**, *24*, 203−206.

DOI: 10.1021/acsomega.8b02804
ACS Omega 2018, 3, 16831−16838